Experimental Procedures for Displacement-Controlled Pure Torsion Tests on Reinforced Concrete Shells

Edvard P.G. Bruun[1], Evan C. Bentz[2]

[1] M.A.Sc. Candidate, University of Toronto
Civil Engineering Department, 35 St. George Street
edvard.bruun@mail.utoronto.ca
[2] Associate Professor, University of Toronto
Civil Engineering Department, 35 St. George Street
bentz@ecf.utoronto.ca

Abstract. Torsion in reinforced concrete structures is a common but complex phenomenon that requires further study, a fact that is reflected in the relative lack of well-documented experimental programs, and empirical and overly conservative provisions in structural design codes. This gap in our knowledge can be partially explained by the difficulty in constructing, executing, and properly documenting torsion experiments - non-standard experimental setups with complex boundary conditions and specimen geometry are often necessary, while the effect of torsion is itself difficult to decouple from flexural and shear effects. To remedy this, a pilot project was launched at the University of Toronto to assess the feasibility of gathering high-quality data on the mechanics of torsion in reinforced concrete. This led to the world's first pure torsion tests (no coupled effects) on two large-scale reinforced concrete shells (1626 x 1626 x 285 mm), one with and one without shear reinforcement, conducted using the Shell Element Tester (SET). Adding to the ground-breaking nature of this work, these tests were also performed in a newly developed and implemented displacement-controlled framework, which allowed for the gathering of stable post-peak data for each specimen. Previously, the SET was run in a force-controlled manner, whereby the 60 servo-controlled actuators were instructed to exert forces that were simply incremented until failure. This experimental program also constituted the most well-documented set of shell tests to date from a data perspective, with both in-plane and out-of-plane instrumentation used to measure the behaviour of the shell throughout the duration of the experiment. In addition to the standard surface-mounted Linear Variable Differential Transformers (LVDTs), a state-of-the-art 3D imaging camera system was used to measure the detailed in-plane surface strains and deformations of the specimen. For the out-of-plane strain measurements, a series of embedded concrete gauges and Linear Potentiometers (POTs) were placed through the thickness of the shell in the planes of the main longitudinal reinforcement.

This paper presents a clear procedure for the construction and instrumentation of the shell specimens, followed by the implementation of the displacement-controlled testing framework used with the SET necessary to achieve post-peak behaviour. The data processing methods for the various types of instrumentation are also explained, with a final discussion on the improvement in strength and ductility for shells in pure torsion resulting from the addition of out-of-plane shear reinforcement.

Keywords: Torsion, Reinforced Concrete, Shell, Displacement Control, Post-Peak.

1. INTRODUCTION TO EXPERIMENTAL PROGRAM

1.1 RESEARCH OBJECTIVE

The objective of this project is to design, construct and carry-out a testing program for two reinforced concrete shells under pure torsion, with the goal of determining the influence of T-head shear reinforcement on the ultimate strength and ductility of the specimens. The testing procedures, instrumentation setup, and the preliminary data analysis from these experiments are presented in this paper. These are the first pure torsion tests ever performed, therefore it was deemed necessary to carefully explain the experimental procedures to serve as a foundation for future tests of this nature.

1.2 SPECIMEN DESIGN AND CONSTRUCTION

The two specimens (ES1 & ES2) were designed as an extension to a previous experimental program undertaken at the University of Toronto [Proestos, 2014; Proestos et al., 2016]. This previous research consisted of a partnership with Seoul National University [Bae et al., 2014], hence the reinforcement ratios and concrete strengths selected in the current study are nominally the same as those typically seen in Korean nuclear containment shell structures (Table 1). Although the percentages used for the current program are higher, the main flexural steel values are comparable when considering the higher strength steel in the Korean shells.

Table 1. Reinforcement Ratios in the APR 1400 Containment Structure [Bae, 2014]

Location	Vertical [%]	Horizontal [%]
Dome	0.56	0.56
Wall (Spring Line)	1.84	1.93
Wall (Mid-Level)	0.66	1.39
Wall (Lower Level)	2.10	1.39

The two specimens presented in this thesis had dimensions of 1626 x 1626 mm square, with a thickness of 285mm. Both specimens had identical orthogonal in-plane longitudinal (X-direction) and transverse (Y-direction) reinforcement arrangements, equivalent to 2.95% and 1.95% of their respective cross-sectional areas. Despite some variation in the concrete strengths, the only significant experimental difference between the two specimens was the additional out-of-plane (Z-direction) T-head reinforcement included in ES2, equivalent to a ratio of 0.32% of the cross-sectional area. Keeping all other parameters constant across the two specimens meant that the effect of the out-of-plane reinforcement could be clearly discerned. The reinforcement spacing, and the resulting percentages are summarized in Table 2.

Table 1. Summary of Specimen Reinforcement

Name	Dimensions [mm]	X-Bars [mm]	Y-Bars [mm]	Z-Bars [mm]
ES1	1626x1626x285	20M @ 72 (2.95 %)	20M @ 108 (1.95%)	-
ES2	1626x1626x285	20M @ 72 (2.95%)	20M @ 108 (1.95%)	#4 @ 200 (0.32 %)

1.2.1 Reinforcement Cages and Casting Specimens

Each specimen was constructed and assembled as two separate but identical reinforcement cages that represented the inner and outer faces of a shell structure (Figure 1). Each cage consisted of a layer of orthogonal X and Y direction reinforcement, but oriented at 45° as shown in Figure 2, which is a schematic drawing of the reinforcement layout for specimen ES2 (ES1 is identical except it has no T-head reinforcement).

Figure 1. Welded Reinforcement Cage (Half Specimen)

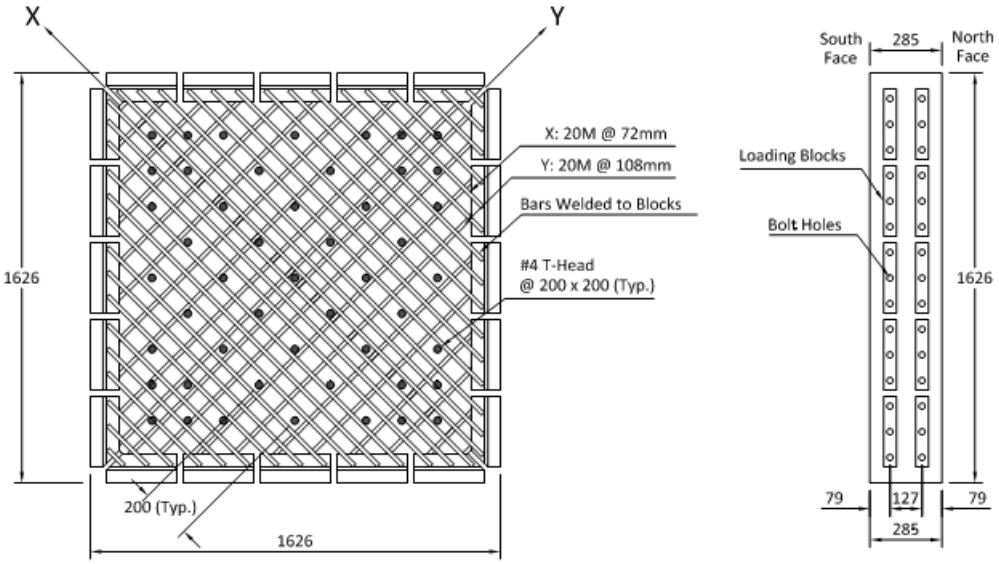

Figure 1. ES2 North Face Cage Reinforcement Layout

Figure 3 shows an assembled specimen ready for casting, with the North and South face cages anchored to the casting forms (Left), and the same specimen after concrete casting, but before fishing of the surface (Right). The hollow tubes sticking through the surface of the specimen are necessary for the out-of-plane instrumentation, which will be discussed further in Section 3.4.

Figure 3. Casting Reinforced Concrete Shell Specimens

Figure 4 shows a finished specimen with a painted surface awaiting the installation of all the in-plane and out-of-plane instrumentation. The holes visible on the surface are required for various mounts to support the instrumentation.

Figure 4. Completed Shell Specimen

1.3 MATERIAL PROPERTIES

The individual stress-strain responses of the steel and concrete components in reinforced concrete are necessary to properly model large-scale structural behaviour. Hence axial tests were performed on steel reinforcement bar coupons and concrete cylinders representative of the materials used to build the shell specimens.

1.3.1 Concrete

Plain concrete cylinders with a diameter of 6" were cast from the same concrete batch as the shell specimens. Both shells were cast on October 5th, 2016 the results from the cylinder tests were used to determine the compressive strength gain curve (Figure 5). The points represent the average of three separate cylinder tests performed at 7, 21 & 28 days after the cast, and on the dates of the shell tests. Specimen ES1 was tested early, slightly before 28 days, since it was concluded that reasonable strength had already been achieved. The concrete compressive strength difference between the two specimens is reasonable for regular strength concrete, and will have to be accounted for when modelling the specimens. Concrete tensile strength was not a critical factor in the tests and was therefore not determined explicitly.

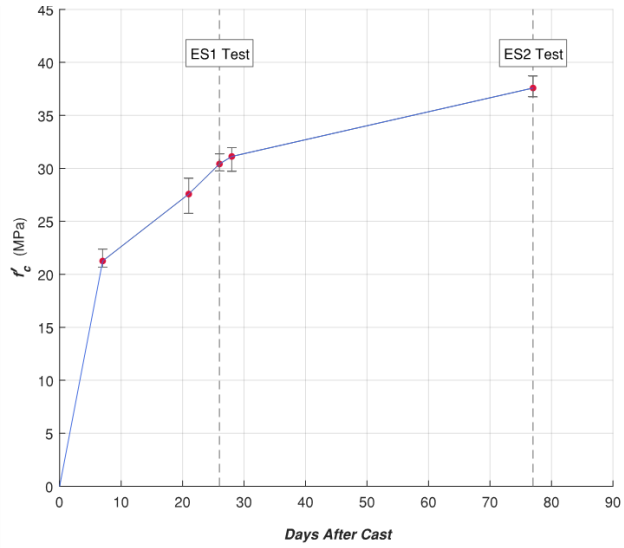

Figure 5. Concrete Compressive Strength Gain

The detailed average peak properties, based on three separate tests, for the concrete on the test days are shown in Table 3.

Table 3. Average Test Day Concrete Properties

Test	f'c [MPa]	e'c [x10^{-3}]
ES1	30.4	1.75
ES2	37.6	1.87

1.3.2 Steel

The average results for the steel coupon tests are shown in Table 4 (three tests per steel type). The longitudinal reinforcement (X and Y directions) was all 20M bars from the same batch, while the out-of-plane reinforcement (Z direction) was in the form of #4 T-head bars.

Table 4. Average Reinforcement Steel Properties

Bar	Area [mm^2]	f_y [MPa]	f_u [MPa]	e_y [x10^{-3}]	e_{sh} [x10^{-3}]	e_u [x10^{-3}]
20M	200	509	636	3.45	15.1	110
#4	129	474	657	2.23	11.5	133

2. SHELL ELEMENT TESTER SET-UP

The experiments were performed with the Shell Element Tester, a unique experimental set-up capable of applying any combination of the eight stress resultants potentially experienced by a shell structure. By varying the loading ratios and the orientation of the longitudinal reinforcement, different combinations of in-plane and out-of-plane shear stresses, axial stresses, and moments can be applied to the appropriate section. The Shell Element Tester consists of servo-controlled actuators operated with the MTS® FlexTest controller interfaced with a computer running the AeroPro™ Data Acquisition System [MTS, 2009], which allows for a high level of control and precision throughout the test. The actuators are connected to the shell specimen through loading yokes bolted to blocks cast into the concrete. For a detailed technical description of the Shell Element Tester and the preparation and installation of a specimen see the work of Dr. Ruggiero, Figure 6 is a schematic of the Shell Element Tester and is adapted from his PhD thesis [Ruggiero, 2015].

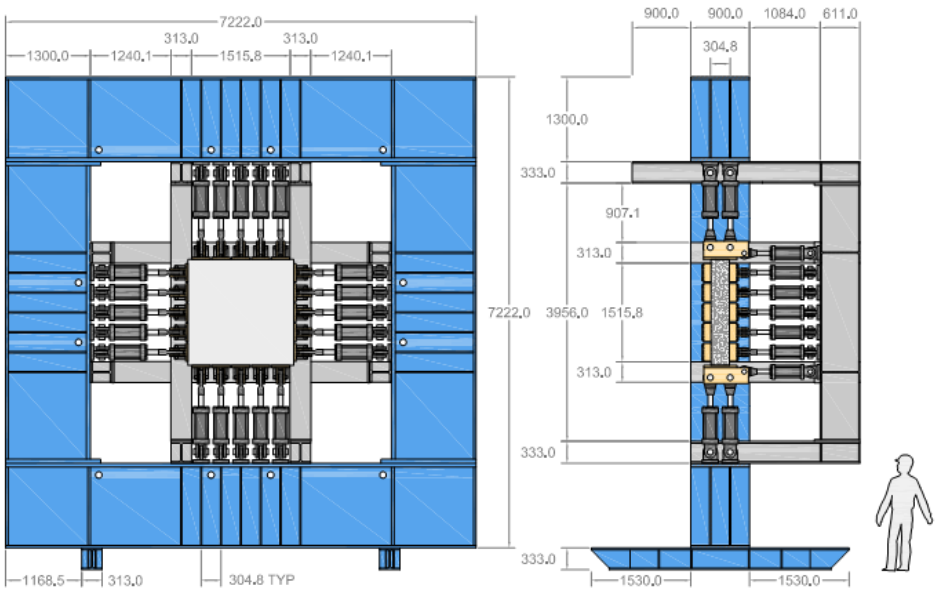

Figure 6. Shell Element Tester Schematic [Ruggiero, 2015]

2.1 ACTUATOR CONFIGURATION AND DISPLACEMENT CONTROL

The Shell Element Tester consists of 60 servo-controlled hydraulic actuators, which are positioned around the four sides of the frame. Each side has 10 in-plane actuators (aligned in two banks of 5), along with 5 out-of-plane actuators. Figure 7 shows the actuator numbering used in the control system, and a 2D representation of their arrangement. For example, the bottom face has in-plane actuators numbered 1-10 (1-5 on the front, 6-10 on the back), and out-of-plane actuators numbered 11-15. To stabilize the specimen and prevent rigid body motion during the test, six of the actuators were placed in displacement control and set to maintain zero displacement. This is analogous to a simply-supported beam, where three restraints are needed to achieve statical determinacy. Fixing fewer points would lead to instability, while fixing more would lead to a statically indeterminate structure. Actuators #21, #25 & #40 (red box) provided the three necessary in-plane restraints, while actuators #11, #15 & #28 (blue box) provided the necessary out-of-plane restraints. Actuator #8 (green box) is the control displacement channel, which is discussed further in the context of the loading protocol in Section 2.3.

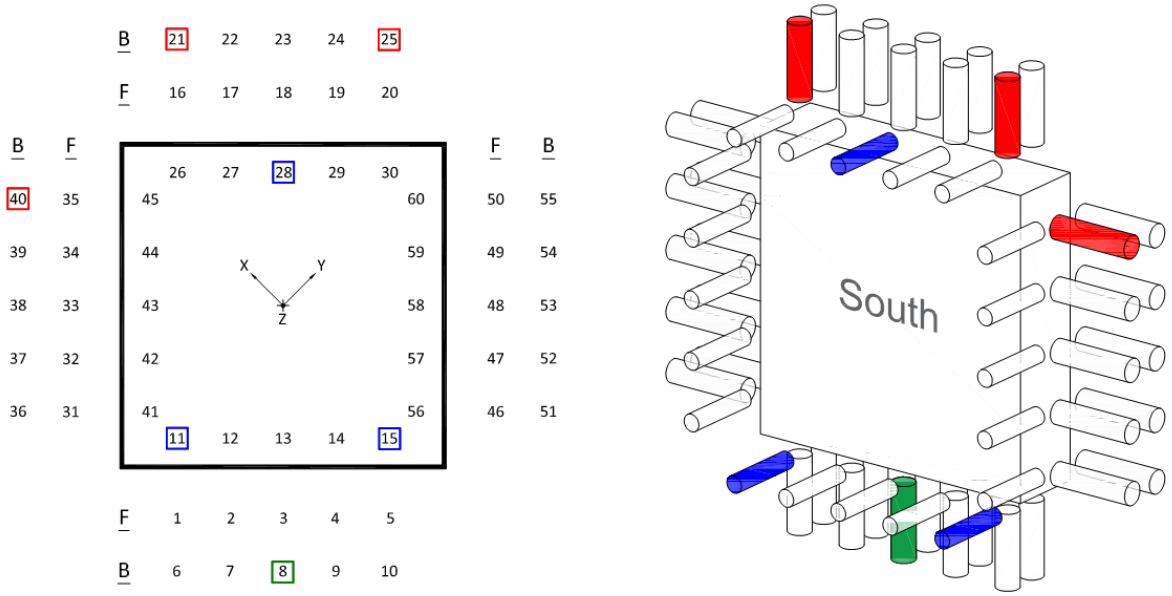

Figure 7. Actuator Placement and Numbering

2.2 COORDINATE SYSTEM

The specimen coordinate system (XY) is rotated 45° to the plane of the actuators (HV), where the XY-plane coincides with the location of the longitudinal reinforcement. The right-hand rule dictates that the +Z direction is taken into the page when looking from the North, which is the case for the left image in the actuator placement figure from the previous section. It is important to note that previous experimental programs using the Shell Element Tester have defined the shell coordinate system differently, so care must be taken when comparing results across sources.

The nature of pure torsion loading, and the placement of the instrumentation, requires one to refer to the North and South face as separate entities at times. In such cases it is critical to keep a consistent coordinate system. Figure 8 depicts the same coordinate systems viewed from either a North or South frame of reference. Subsequent discussion in this paper will be consistent with this notation.

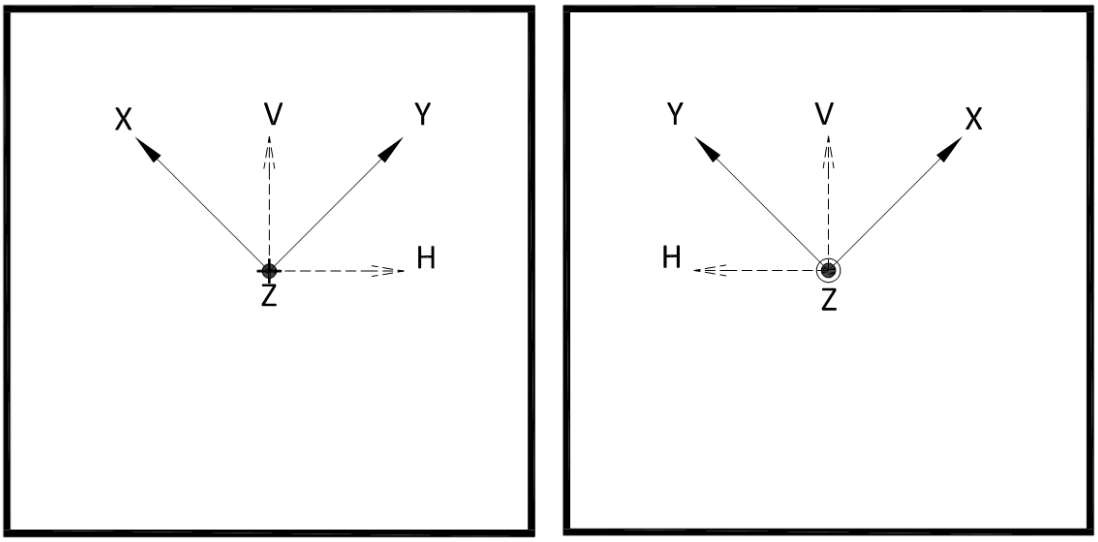

Figure 8. Shell Element Coordinate System (Left = North, Right = South)

2.3 LOADING PROTOCOL

In both experiments only the 40 in-plane actuators were necessary to apply pure torsion to the shell specimen. The three out-of-plane rigid links were active to provide the necessary static restraint, but the remaining out-of-plane actuators were simply set to a constant ±5 kN of force during the test to further stabilize the shell and prevent buckling. These experiments were effectively in-plane tests, so for clarity the out-of-plane actuators are not included in subsequent images detailing the loading protocol.

2.3.1 Displacement Control

Both experiments were performed in a displacement control mode, which is a new development in the capabilities and usage of the Shell Element Tester. All previous tests have been force controlled, which meant that the user simply controlled and incremented the forces in the actuators until the specimen failed. Although this simplied the execution of the test, it did not allow for any post-peak behaviour and could on occasion lead to sudden and dangerous specimen failures.

A displacement control test is much more complicated to implement and execute, but allowed for accurate post-peak behaviour and user controlled load-shedding once the test was completed. In this experimental program, the master displacement was assigned to actuator #8; the displacement on this channel is increased as the test progressed, and the load that was developed to achieve the target displacement on this actuator was used as the input for all other actuators.

2.3.2 Pure Torsion in Shells

To apply pure torsion in the XY-plane, moments of equal magnitude and opposite sign were applied along the H & V edge of the shell. In the Shell Element Tester, moments are applied by setting one bank of actuators into tension, while simultaneously setting the adjacent bank to compression. In these tests, the magnitude of the compression and tension along one face was kept equal, resulting in a pure couple with no net axial force. Figure 9 shows the sign of the force in each of the in-plane actuators throughout the test, while Figure 10 shows the same loading condition represented on both the North and South faces respectively.

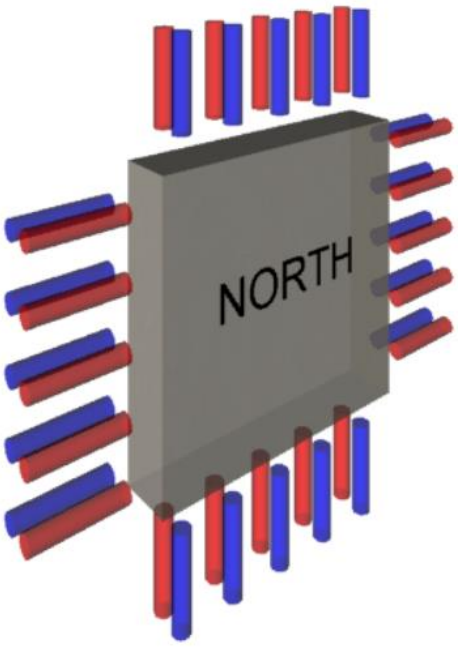

Figure 9. In-Plane Actuator Forces During Test (Red = Tension, Blue = Compression)

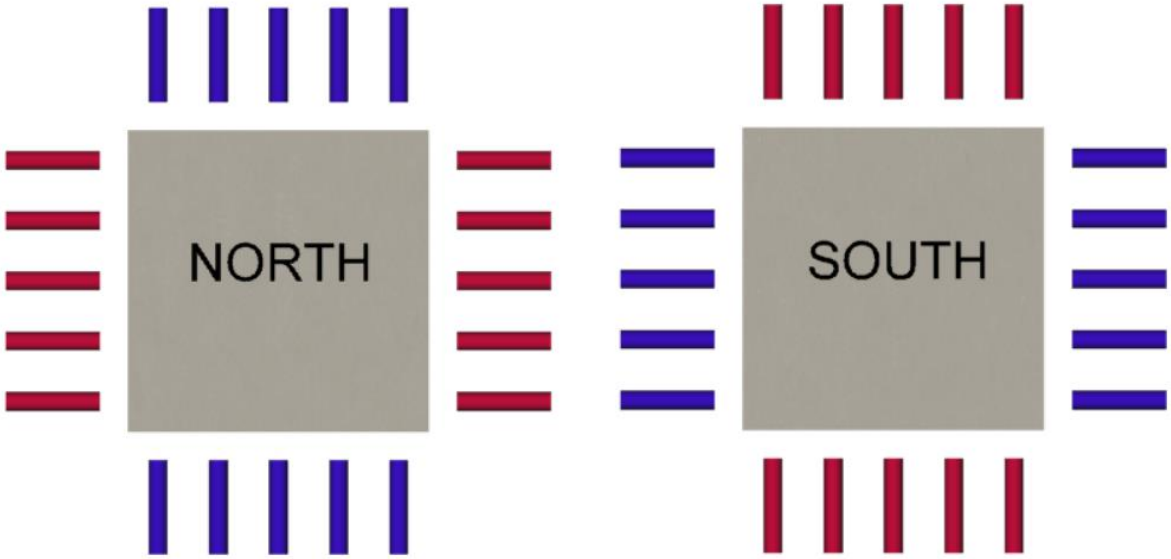

Figure 10. In-Plane Actuator Forces on North/South Face (Red = Tension, Blue = Compression)

The Shell Element Tester can only apply axial forces in the H & V directions. Yet the actual test region is defined by the orthogonal axis of the longitudinal reinforcement, which is rotated 45° to the HV-plane. The square element (XY-plane) inscribed inside the full shell specimen in Figure 11 represents the test region.

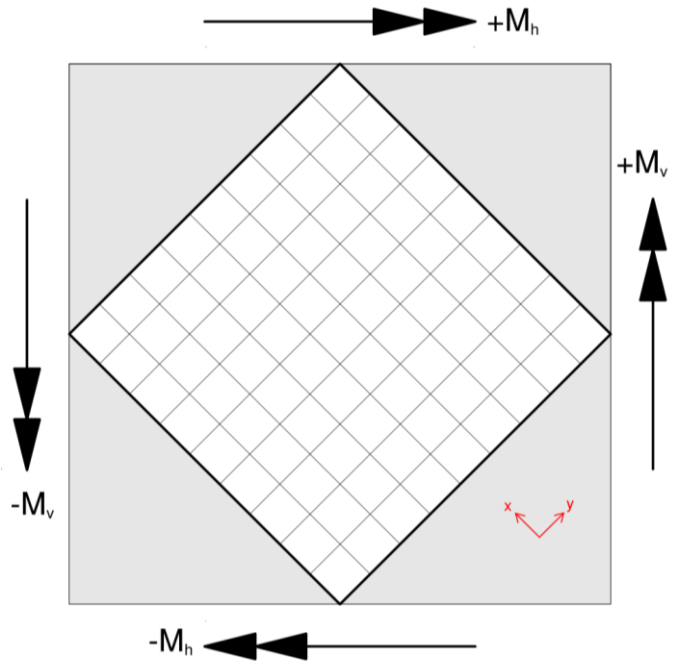

Figure 11. External Moments Applied to the Specimen (Viewed from North)

Resultants can be found by satisfying static equilibrium at the boundaries of the test region. This calculation is straightforward as the internal cut is at 45°, and the magnitudes of external moments on adjacent faces are equal (i.e. $|M_h| = |M_v|$). Figure 12 shows the free-body diagram of the resultant moment on the test region. The external moments clearly result in pure torsion on the test region (XY-plane), where the magnitudes of torsional moments on adjacent faces are equal (i.e. $|M_{xy}| = |M_{yx}|$).

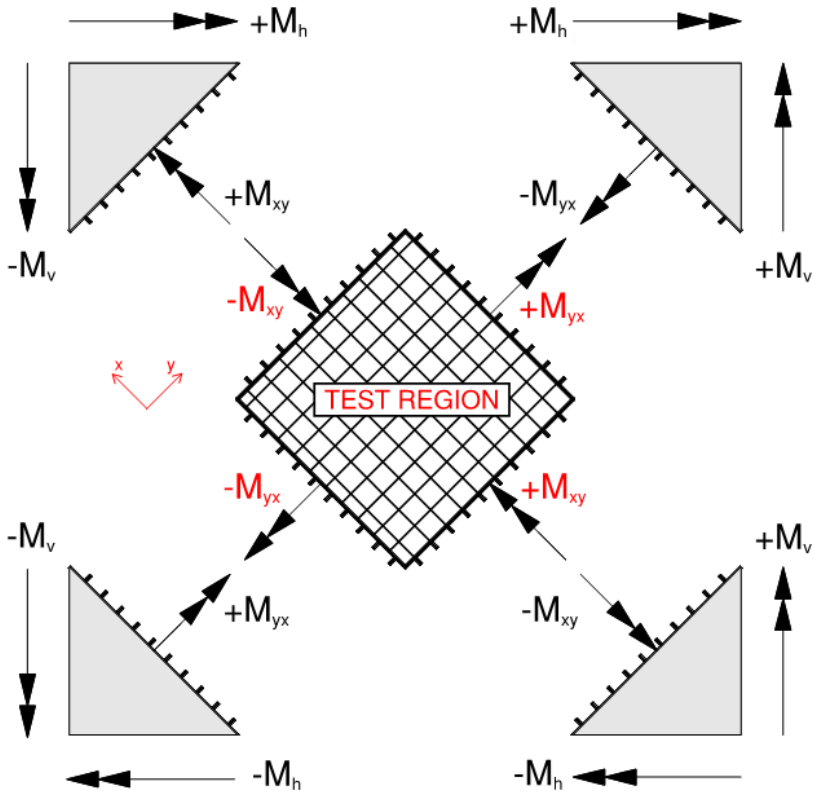

Figure 12. Pure Torsion Applied to the Test Region

Pure torsion can also be thought of as a couple resulting from pure in-plane shear forces on the North and South faces respectively. Figure 13 shows both faces of the shell as viewed from the North, the moment created by the shear forces is equivalent to the torsion on the test region (direction and magnitude).

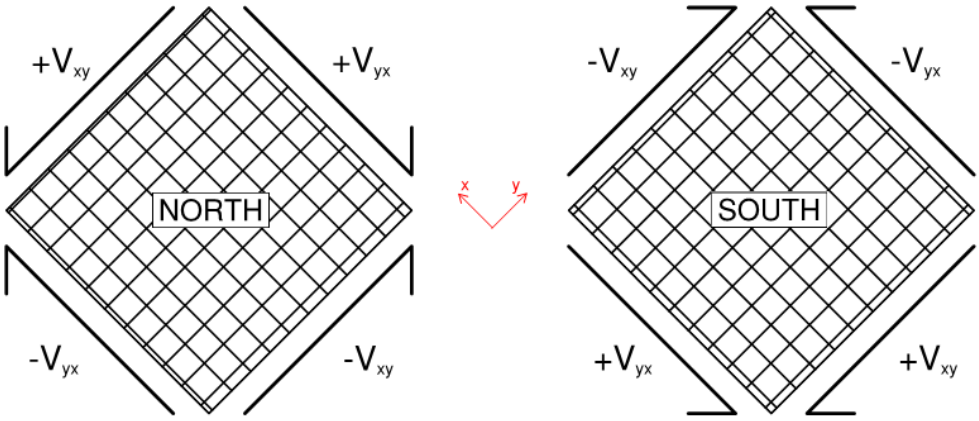

Figure 13. Torsion Represented as In-Plane Shear Forces (Viewed from the North)

3.INSTRUMENTATION

The Shell Element Tester actuators come equipped with displacement and force sensors, but to improve the quality of data gathered additional surface and embedded measurement devices were included with the specimens. There were two main data streams for these external devices: the force and strain/displacement data routed through the AeroPro™ Data Acquisition System (DAQ), and the 3D surface coordinate data captured by the Nikon® (formerly Metris) metrology system. The following sections will outline the placement and orientation of the additional instrumentation used in both experiments; to establish data consistency across the tests both ES1 & ES2 were instrumented in the same manner.

3.1 BUILT-IN ACTUATOR SENSORS

Each of the 60 actuators on the Shell Element Tester had its own built-in sensors capable of providing continuous data: a load cell to measure the force exerted, and an external string potentiometer to measure the displacement. The proper functioning of these sensors was of critical importance to the test, as they provided information regarding the external loading and experimental execution. For example, the string potentiometer for actuator #8 was used as the master control channel for the whole test, while the six string potentiometers on the rigid link actuators had to be kept at zero displacement throughout the test to ensure stability. Accurate load cell readings from the in-plane actuators were also used to determine the magnitude of torsion being applied to the shell specimen during the test.

3.2 LINEAR VARIABLE DIFFERENTIAL TRANSFORMERS (LVDTS)

To measure average in-plane strains, six LVDTs were mounted on both the North and South face of the specimen: two horizontal, two vertical, one in the X-direction, and one in the Y-direction. Figure 14 shows the placement of the LVDTs on the specimen, both faces are shown from the North (i.e. the South face is an x-ray view through the specimen). The diagonal LVDTs on the South face are slightly shifted to avoid interfering with the 3D coordinate measurement system. The naming convention used is as follows: 1st letter = face, 2nd letter = measurement direction, 3rd letter = relative locations.

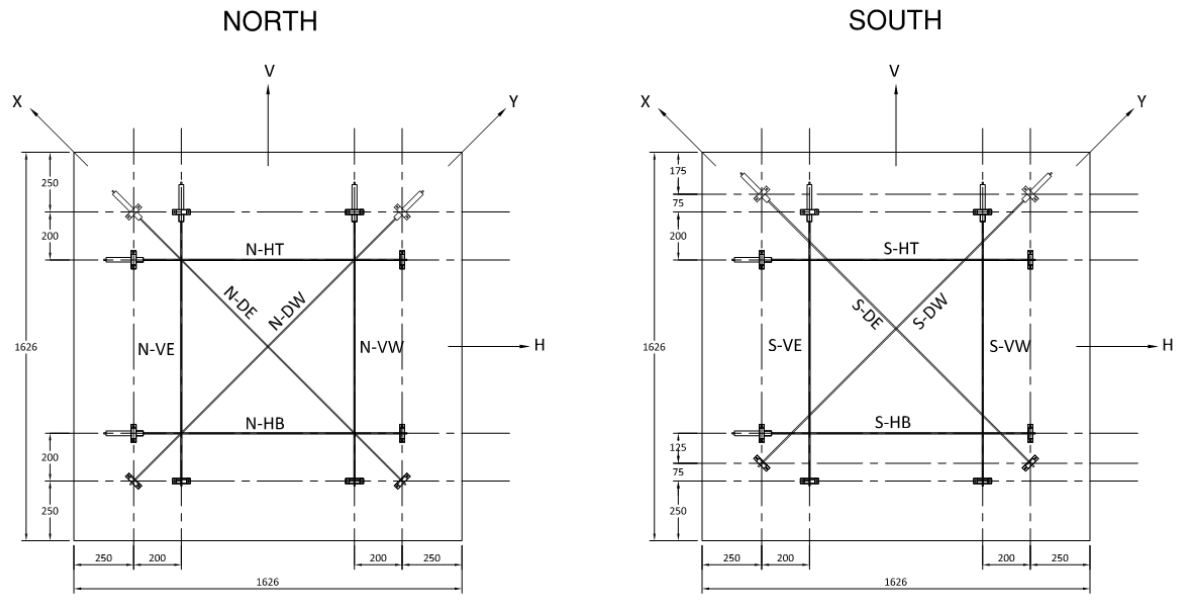

Figure 14. In-Plane LVDT Locations (Viewed from North)

To fully define a Mohr's circle of strain (i.e allowing one to calculate the full strain state in any 2D plane) three independent axial strain measurements at known angles are necessary. This is achieved by using three of the LVDT measurements, oriented in any direction, to explicitly calculate the size and position of the Mohr's circle. This means that one of the directions in our four LVDT set-up is not necessary (the Mohr's circle is considered over-defined) and is typically discarded to reduce it to a three-strain system that can be explicitly calculated (Left, Figure 15). But rather than waste useful data, the Mohr's circle calculations in this research use a procedure that has been developed (Appendix, Ruggiero, 2015) to determine a Mohr's circle of "best-fit" using all four measurements while minimizing the overall error (Right, Figure 15).

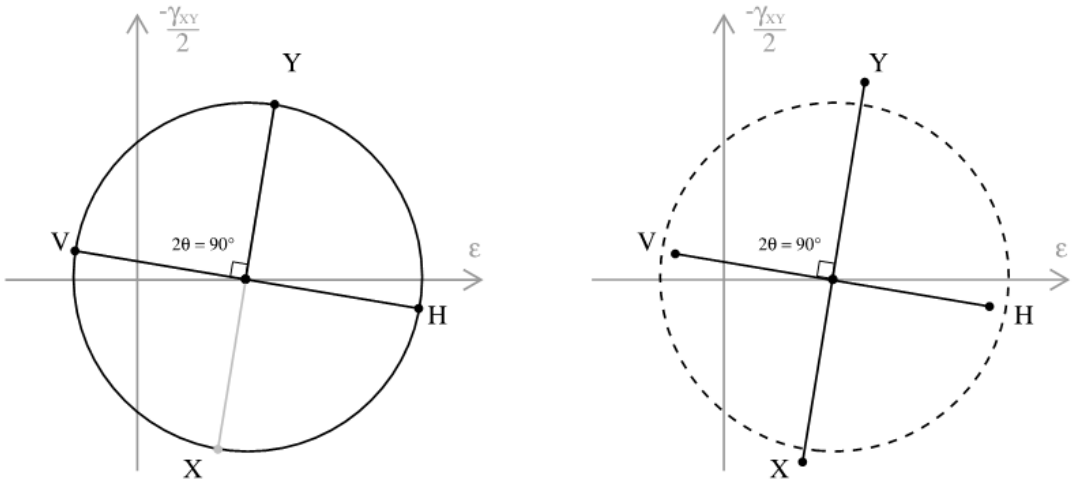

Figure 15. Fully Defined Mohr's Circles (Left = Three-Strain, Right = Best-Fit)

3.3 3D COORDINATE MEASUREMENT SYSTEM

Surface displacements and in-plane strains on the South face were measured using a three-dimensional position tracking system, which consisted of an infrared camera coupled with infra-red light emitting diode (LED) targets. The positions of the LEDs was recorded throughout the test using the Metris software sampling at 10 Hz, which was later synchronized with the data stream from the AeroPro™ Data Acquisition System (DAQ).

In both tests a 6 x 6 rotated square grid of LEDs (total of 36) was placed to subdivide the test region into 25 equal sized elements (200 mm x 200 mm). Figure 16 shows the placement and numbering of the LED targets and the resulting elements (red text) as seen from the South. The LED displacement data is useful since it allows both a qualitative look at the three-dimensional displaced shape of the shell, and detailed in-plane strain measurements over the test region. The LVDTs are providing the same type of in-plane data as the LEDs, but are doing so over the whole surface of the shell and cannot therefore represent localized behaviour. Meanwhile, each square LED element can act as its own independent measurement system. The Mohr's circle of strain can be calculated for each of the 25 LED elements, allowing a look at the South face in-plane strain on a finer spatial scale.

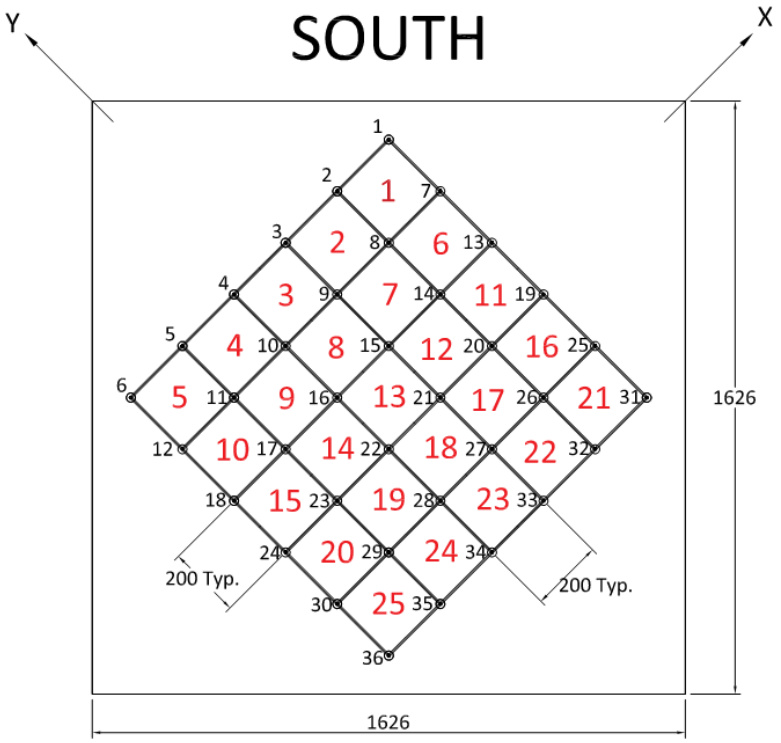

Figure 16. In-Plane LED Locations (Viewed from South)

3.4 LINEAR POTENTIOMETERS (LPS)

A total of 15 LPs were used to determine the out-of-plane strains over the full thickness of the shell. Hollow PVC pipes, which are visible during construction (Figure 3), were tied to the reinforcement cage and cast into the concrete at the specified locations. These embedded tubes provided a clear path through the shell, allowing the LPs to measure the relative strain between the North and South face. The LPs were placed inside the test region, organized in sets of three along the orthogonal reinforcement directions. Three LP triplets (total of nine) were placed in the Y-direction, and two LP triplets (total of six) were placed in the X-direction. In each set, one LP was placed directly through the thickness (Z-direction), while the remaining two were inclined at roughly ±45° to either the XZ or YZ planes as seen in Figure 17. Three independent strain readings at known directions provide enough information to define the complete Mohr's circle of strain over this area.

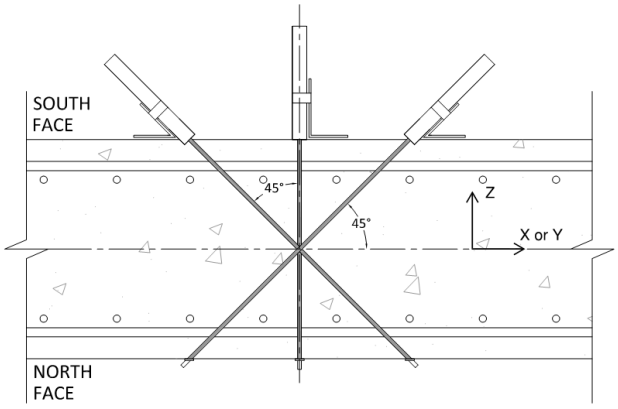

Figure 17. LP Through-Thickness Placement

Figure 18 is a schematic of the LP locations on the South face of the shell. The central Y-direction triplet is slightly shifted to avoid interfering with the 3D coordinate measurement system.

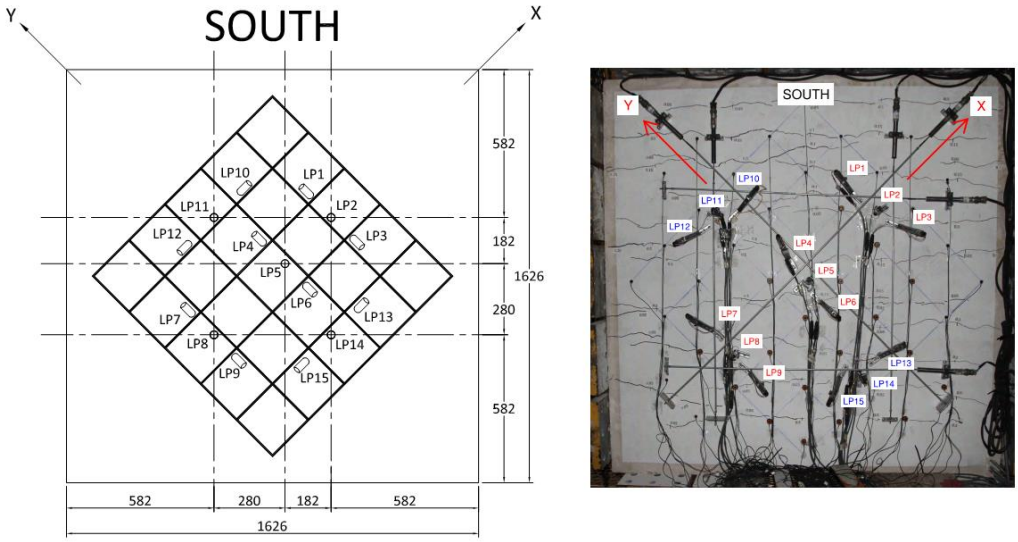

Figure 18. LP Placement on Specimen ES1

3.5 EMBEDDED CONCRETE STRAIN GAUGES (EGS)

Four EGs (PML with 60 mm gauge length) were used in each specimen to complement the out-of-plane measurements from the LPs. The EGs work on the same principal as the LP triplets, except in their case the three separate gauges are pre-arranged and fixed into a 45° rosette as shown in Figure 19. The main difference between the EGs and LPs, is that the EGs are fully encased in concrete and only define the Mohr's circle of strain at a localized internal point, while the LPs define the Mohr's circle of strain over the whole thickness of the shell. An internal local concrete crack has the chance of occurring right across one of the individual gauges; such an occurrence would either cause the gauge to fail or skew the resulting Mohr's circle in an unrealistic way, both options effectively rendering the EG data useless. Hence relying on the EGs for more than simple verification is not recommended.

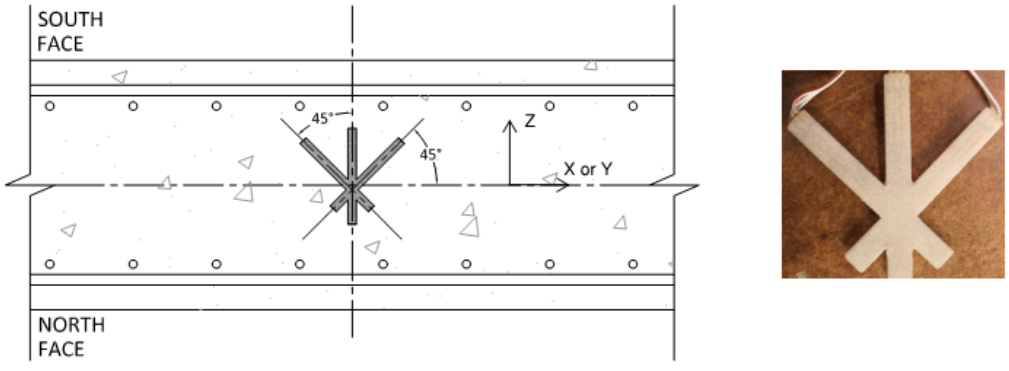

Figure 19. EG Through-Thickness Placement

Figure 20 is a schematic of the four EG locations inside the test region. Two of the EGs are oriented in the XZ plane, and the remaining two are oriented in the YZ plane. The naming convention simply indicates in which plane the EG is placed.

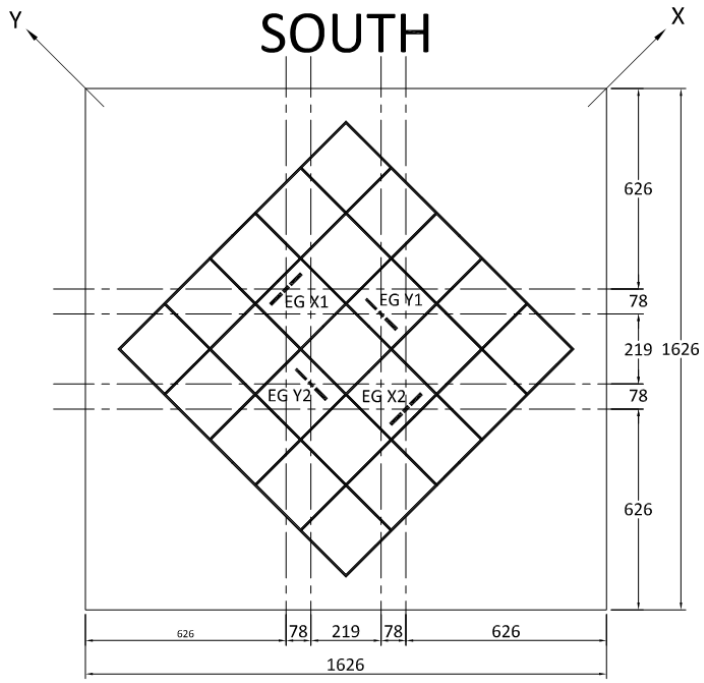

Figure 20. Out-of-Plane EG Locations (Viewed from South)

The EGs are placed as close as possible to the center of the shell between the North and South faces, and in the direction of the longitudinal reinforcement. Figure 21 shows a shell specimen cage before casting, with the EGs located just below the level of the top reinforcement. The hollow PVC ducts, which are necessary for the installation of the LPs, can be seen extending through the thickness of the shell.

Figure 21. Out-of-Plane Instrumentation in Reinforcement Cage

3.6 REINFORCEMENT STRAIN GAUGES (SGS)

To measure reinforcement strains during the test, each specimen had 20 foil SGs (FLA with 5 mm gauge length) placed on several longitudinal bars in the test region. These gauges were equally divided between the North and South cages: 6 in the Y-direction, and 4 in the X-direction per cage. Figure 22 is a schematic of the SG locations on the South reinforcement cage, the North face cage is identically instrumented. The naming convention used is as follows: 1st letter = face, 2nd letter = direction, 3rd letter = relative location.

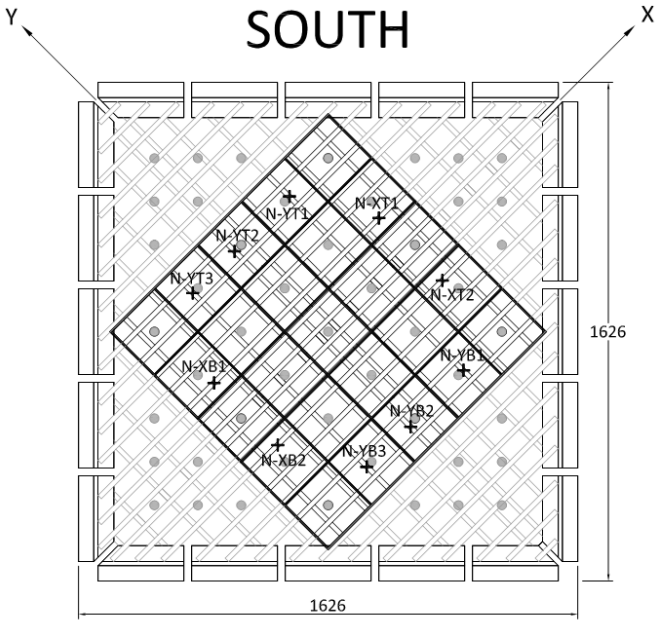

Figure 22. Longitudinal Bar SG Locations (Viewed from South)

Specimen ES2 had an additional 8 SGs, each placed in the center of an out-of-plane T-head reinforcement bar located in the test region. Figure 23 shows which T-head bars were instrumented.

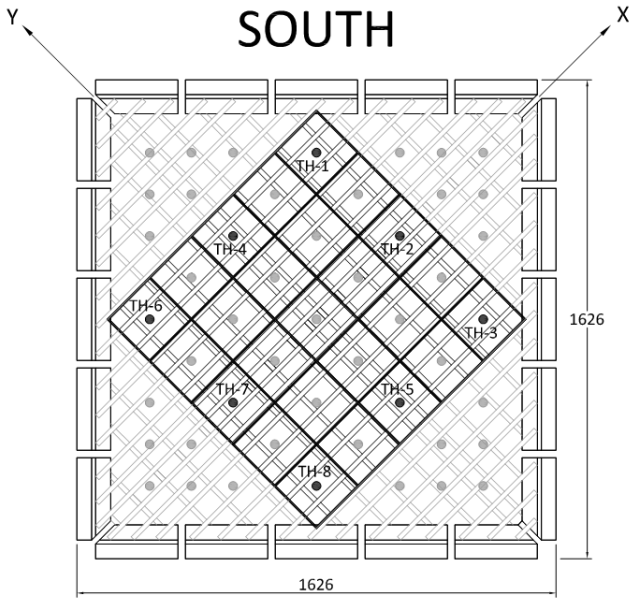

Figure 23. T-Head Bar SG Locations in ES2 (Viewed from South)

4. EXPERIMENTAL OBSERVATIONS AND RESULTS

4.1 EXPERIMENTAL PROGRESSION

Figure 24 presents the high-level behaviour of both specimens in the form of the applied torsion in relation to the twist strain. The two specimens initially exhibit the same cracked stiffness, which was expected since their concrete strengths and longitudinal reinforcement ratios were the same. Although ES1 begins to soften towards its peak torsion point, deviating from the linear stiffness. The addition of T-head reinforcement has a significant impact on both the strength and ductility of specimen ES2, an improvement over ES1 of 33.8% and 52.2% respectively. While the experimental variability typical in reinforced concrete could possibly accounts for some of the variation, the magnitude of the difference implies that there is an inherent benefit in including T-heads. The post-peak stiffness is similar as in this region as cover spalling continues to develop in both specimens.

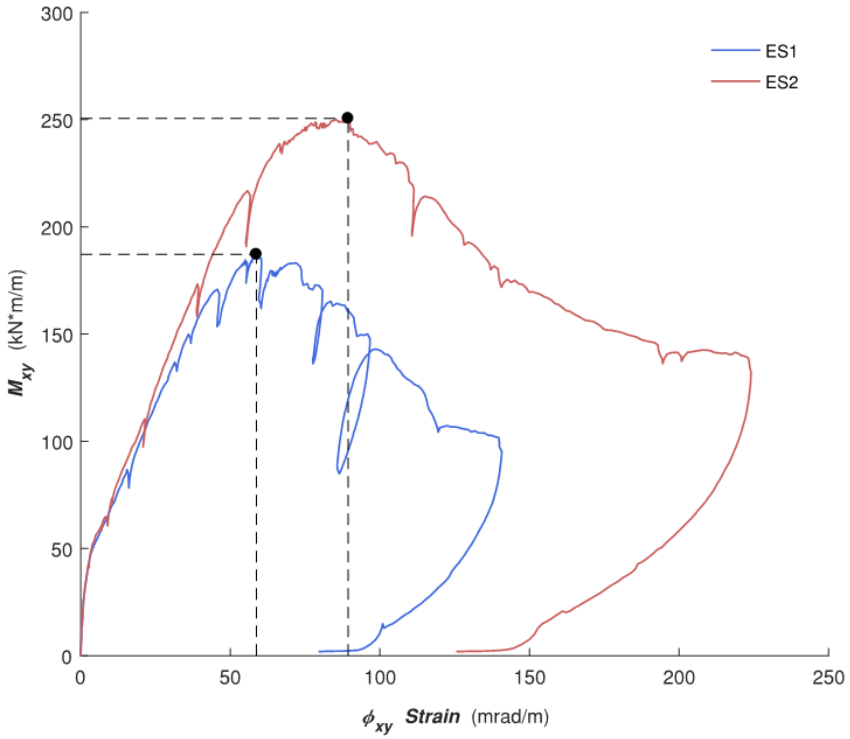

Figure 24. Applied Torque-Twist Comparison

The values at the load stages for both experiments are summarized in Table 5.

Table 5. Experimental Load Stages (Left = ES1, Right = ES2)

	M_{xy}	φ_{xy}		M_{xy}	φ_{xy}
LS 1	86.8	15.5	LS 1	64.8	8.2
LS 2	168.8	46.3	LS 2	110.5	21.4
Peak	187.2	58.7	LS 3	173.4	39.0
LS 3	182.9	60.4	LS 4	214.7	56.7
LS 4	170.4	80.8	Peak	250.5	89.4
LS 5	147.9	96.6	LS 5	219.6	111.0
LS 6	101.8	139.7	LS 6	138.9	223.0

4.2 SPECIMEN DEFORMATION AND DAMAGE

Since shears stresses of opposite signs were being applied on the North and South faces, the directions of the cracks on the specimens were expected to be oriented at 90° to each other. Figure 25 shows the North and South face for specimen ES1 at failure, where the directions of the cracks are seen to be vertical and horizonal respectively. ES2 exhibited the same behaviour.

Figure 25. Specimen ES1 at Failure (Left = South, Right = North)

In general, the specimens failed by crushing of the outermost concrete, and the subsequent spalling of the cover due to the relative torsional deformations across the North and South faces. Figure 26 shows the middle of the test region, where cores were extracted after completion of the experiment to better observe the interior damage. The surface concrete, at the elevation of the top layer of reinforcement, is clearly separated from the rest of the specimen. Four of these probes were made throughout the test region in both specimens, with the same observation at each location.

Figure 26. Visible Cover Spalling at Cored Locations

Looking more closely at the deformations and the type of damage sustained clarifies the behaviour of the specimens. Using the position data from the LED target system provides further evidence of signicant cover spalling between the peak and final load stages. In Figure 27, the initial position of the LEDs is represented by the grey plane, while the new position at either the 'Peak' or 'Final' load stage for specimen ES1 is shown in red; the corresponding point on the torque-twist plot is also shown for reference.

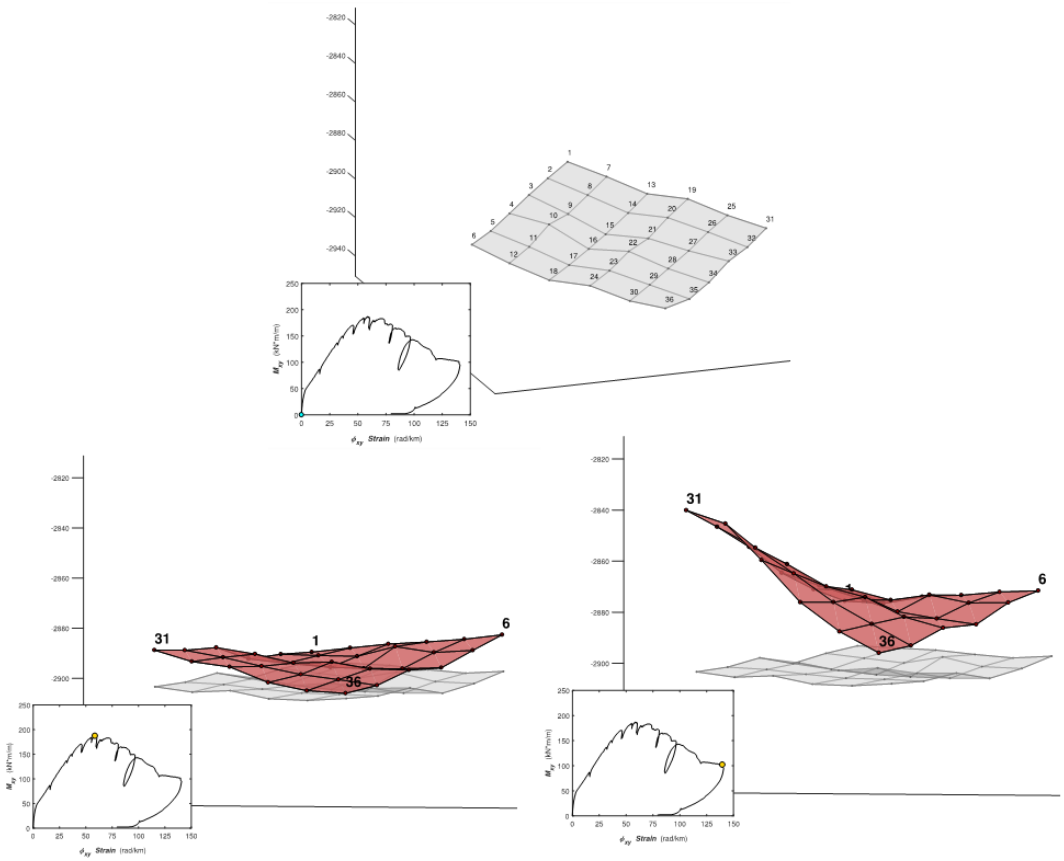

Figure 27. ES1 Surface Deformations Measured by LED Targets (Left = Peak, Right = Final)

4.3 OUT-OF-PLANE MEASUREMENTS

The data gathered by the LPs and EGs shows that there are significant deformations in the out-of-plane direction in both specimens, which was the behaviour this experimental program was designed to investigate. The flattening of the shear strain curves, which is due to the cracking and relative separation of the North and South faces of the shells, clearly prefaces the peak loads in both experiments. As the out-of-plane shear strain in the core increases, ES1 weakens and the peak load is reached as the cover begins to spall shortly after. Meanwhile, ES2 exhibits similar behaviour up to the point where ES1 fails, but has a stiffer response beyond this. The specimen is clearly softening beyond this point, but does so in a much more gradual manner resulting in a higher peak torsion. An explanation for this is that the out-of-plane T-head reinforcement provides additional resistance to the core of the specimen, giving the specimen as a whole more capacity in resisting the out-of-plane deformations and delaying the core failure and subsequent cover spalling.

The data from the EGs and LPs is shown separately (Figure 28) since including them in the same average would beforcing a false equivalency. While they both measure the deformations in the XZ and YZ planes, they do so at different scales: the EGs measure the strains at a point in the core of the specimen, while the LPs measure the strains across the whole width of the specimen. For example, as the cover concrete begins to spall the LPs will record a deformation that will not be captured by the EGs located in the core of the specimen. This difference is clearly manifested in the data when comparing the the pre-peak and post-peak regions. The ratio of the LP/EG strain at the point where flattening of the curves begins (indicating that failure is imminent) occurs at 2.19 and 1.62 for ES1 and ES2 respectively. Looking one load stage into the post-peak region these ratios have increased to 3.07 and 2.18 for ES1 and ES2 respectively.

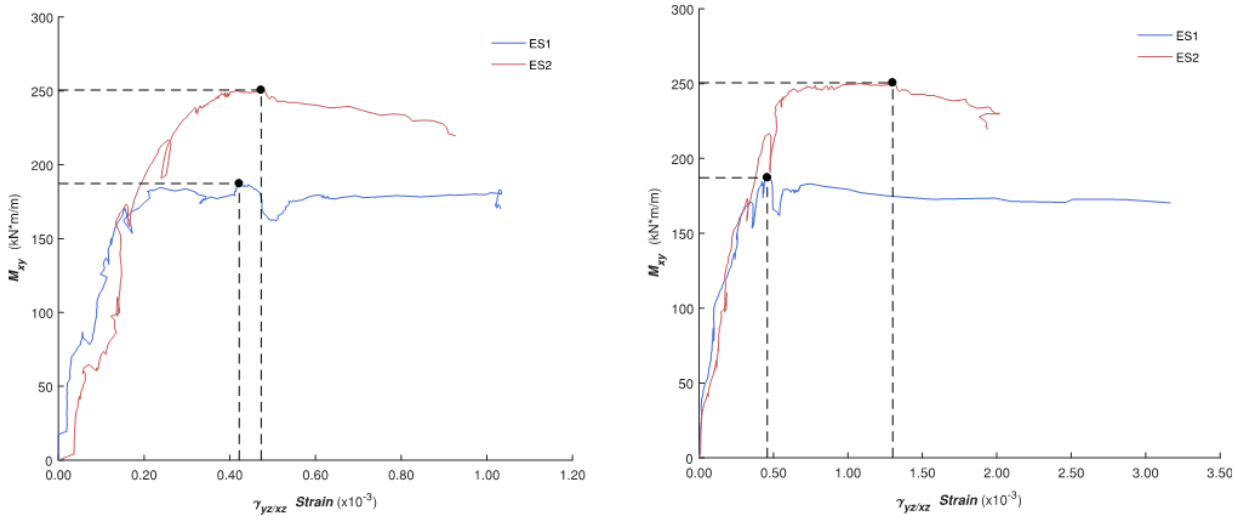

Figure 28. Out-of-Plane Shear Strain Comparison (Left = EGs, Right = LPs)

A critical piece of information gathered from the testing of ES2 were the strains measured in the out-of-plane T-head reinforcement (Figure 29). While only 4 out of the 8 strain gauges were functional during the experiment, they were enough to show that these reinforcement bars played an active part in improving the capacity of the specimen. The strains at the peak are similar to the those measured in the concrete by the EGs, indicating that the strains in the core of the specimen were consistently measured. The reinforcement in the Z-direction continues to develop strain in the post-peak region of the test. This suggests that the post-peak deformations in the specimen are concentrated in the relative separation of the North and South faces of the specimen.

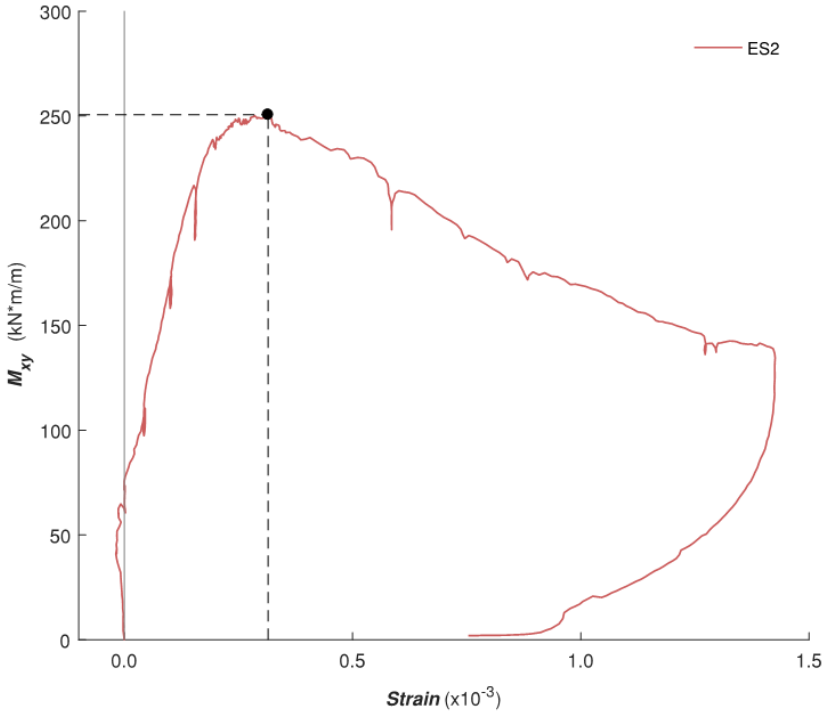

Figure 29. Out-of-Plane T-Head Reinforcement Strain

5.CONLUSIONS

The preliminary data analysis presented in this paper proves that there are significant out-of-plane effects in reinforced concrete shells when tested in pure torsion. This also dispproves one of the initial hypotheses that the T-head reinforcement would have no effect on the capacity of the specimens since no out-of-plane shear forces were directly applied. With respect to the experimental program presented, which consisted of constructing and testing two shell specimens in pure torsion, the following conclusions can be made:

i. A pure torsion loading condition can be recreated in the central test region of a shell by applying equal and opposite moments along the edges of the specimen while orienting the main longitudinal in-plane reinforcement at 45° to the loading axis.
ii. The displacement-controlled loading protocol established for these tests is a viable means of obtaining useful post-peak data from an experiment.
iii. The addition of out-of-plane reinforcement, in the form of T-head bars, significantly improved the strength and ductility of the second shell tested.
iv. Out-of-plane strains and expansion through the thickness of the specimens are important factors to consider when modelling torsion in shells.
v. The specimens experienced crushing of the outermost layers of concrete, due to equal and opposite in-plane shear stresses on the front and back faces. Significant cover spalling occurred in the post-peak region of both tests.

6. ACKNOWLEDGMENTS

The authors would like to thank the Natural Sciences and Engineering Research Council (NSERC) of Canada for the Collaborative Research and Development (CRD) grant that made this overall project possible. On a personal basis, the support from an NSERC Canada Graduate Scholarship (CGS-M) and Ontario Graduate Scholarship (OGS) was an important financial contribution.

The assistance from the University of Toronto's structural laboratory staff was also invaluable in completing the experimental component of this research.

REFERENCES

Bae, Gwang Min. [2014]. "In-Plane Shear Behaviour of Reinforced Concrete Elements with High-Strength Materials." MASc, Korea: Seoul National University.

Bae, Gwang Min, Jae Hyun Park, Jae Yeol Cho, Giorgio T. Proestos, Evan C. Bentz, and Michael P. Collins. [2014]. "Investigation of Shear Response of Nuclear Power Plant Wall Elements Using High Strength Materials." *IABSE Reports* 102 (30): 867–73.

MTS. [2009]. *AeroPro Software Reference*. Version 6.20. MTS System Corporation.

Proestos, Giorgio T. 2014. "Influence of High-Strength Reinforcing Bars on the Behaviour of Reinforced Concrete Nuclear Containment Structures Subjected to Shear." MASc, Toronto: University of Toronto.

Proestos, Giorgio T., Gwang Min Bae, Jae Yeol Cho, Evan C. Bentz, and Michael P. Collins. [2016]. "Influence of High-Strength Bars on Shear Response of Containment Walls." *ACI Structural Journal* 113 (5): 917–27.

Ruggiero, David M. [2015]. "The Behaviour of Reinforced Concrete Subjected to Reversed Cyclic Shear." PhD, Toronto: University of Toronto.